Scanning Electron Microscopy

Volume 1986
Number 3 *Part III*

Article 18

8-15-1986

Integrated Image and X-Ray Microanalysis of Hepatic Lysosomes in a Patient with Idiopathic Hemosiderosis Before and After Treatment by Phlebotomy

M. I. Cleton
University of Utrecht

J. M. Roelofs
State University Hospital

C. J. G. Blok-Van Hoek
Tracor Europa

W. C. De Bruijn
University of Rotterdam

SCANNING ELECTRON MICROSCOPY/1986/III (Pages 999-1006)
SEM Inc., AMF O'Hare (Chicago), IL 60666-0507 USA

0586-5581/86$1.00+05

INTEGRATED IMAGE AND X-RAY MICROANALYSIS OF HEPATIC LYSOSOMES IN A PATIENT WITH IDIOPATHIC HEMOSIDEROSIS BEFORE AND AFTER TREATMENT BY PHLEBOTOMY

M.I. Cleton[I], J.M. Roelofs[II], C.J.G. Blok-Van Hoek[III] and W.C. De Bruijn[IV*]

I. Institute of Pathology, Electron Microscopy Unit, University of Utrecht, The Netherlands.
II. Department of Medical Physics, State University Hospital, Utrecht, The Netherlands.
III. Tracor Europa, Jan van Eycklaan 10, 3720 AH Bilthoven, The Netherlands.
IV. Laboratory for Experimental Electron Microscopy, University of Rotterdam, and Laboratory for Electron Microscopy, University of Leiden, The Netherlands.

(Received for publication March 10, 1986, and in revised form August 15, 1986)

Abstract

Morphometrical and X-ray elemental information was extracted from Scanning Transmission Electron Microscopy (STEM) images of hepatic lysosomes of a patient with idiopathic hemosiderosis before and after treatment by phlebotomy. The elements of interest were (i) iron, stored in pathological quantities in hepatic lysosomal structures and (ii) cerium, used as a capture ion after a cytochemical reaction to detect acid phosphatase activity in the lysosomal structures.

Morphologically the lysosomal structures are heteromorph and the elements iron and cerium are heterogeneously distributed. With "reduced raster" (= reduced scanning area) analysis at 16 x 16 pixelpoints (integrating image and X-ray microanalysis), a marked difference in the area of the cross sectioned lysosomal structures before and after treatment could be demonstrated. Simultaneously the difference in the relative orientation of the elements iron and cerium before and after phlebotomy could be visualized.

Chelex ion exchange beads, loaded with 11.5% w/w iron, and coembedded with the tissue blocks, were used as an internal standard. A mean iron peak to background ratio was obtained and a factor, converting ratio to absolute iron concentration, was calculated. The same calculation procedure, now per pixelpoint, was followed for the hepatic lysosomal structures. A marked difference in iron concentration in the individual lysosomal structures was observed before and after treatment by phlebotomy.

KEY WORDS: Chelex standard, electron microscopy, X-ray microanalysis, image analysis, iron storage disease, lysosomes, acid phosphatase reaction, Fe concentration.

* Address for correspondence:
W.C. de Bruijn
Laboratory for Electron Microscopy
University of Leiden, Rijnsburgerweg 10
2333 AA Leiden, The Netherlands.
Phone no. 31.71.148333, ext. 4666.

Introduction

Recently, using electron probe X-ray microanalysis (EPMA) in situ on ultrathin sections of liver biopsy tissue of patients with iron overload, the presence of ferritin-iron in cytoplasm, lysosomal structures and bile canaliculi has been demonstrated (2). With the same technique an iron to phosphorus ratio has been established in preparations of purified human liver ferritin and horse spleen ferritin. This ratio correlated remarkably well with that calculated from data obtained by chemical analysis. Furthermore, Fe to P ratios in hepatic lysosomal iron storage compounds were determined in patients with various iron storage disorders. These ratios were compared before and after treatment of the patients by phlebotomy (3).

In another study on hepatic lysosomal structures in situ the presence of cerium has been demonstrated by EPMA. Cerium is deposited as a capture ion, after a lysosomal acid phosphatase reaction (7). The simultaneously acquired data on iron and cerium net intensity values in patients with different grades of iron overload and in patients before and after treatment by phlebotomy were compared. To this purpose the material was analysed with multiple point analysis under carefully controlled conditions, such as a controlled beam intensity, spot diameter and acquisition time. These conditions were tested on an internal standard, being iron loaded chelex ion exchange beads (5), coembedded with the tissue blocks and present in the same ultrathin sections. In these studies the elemental distribution in the hepatic lysosomal structures was assumed to be homogeneous, although the authors were aware that this was not the case.

In another study the heterogeneity - with respect to the elements iron and cerium - of hepatic lysosomal structures of patients with iron storage disorders has been established with reduced raster X-ray microanalysis (4). The mean acquired net intensities for these elements, present in the individual lysosomal structures and the lysosomal population, were compared with data, obtained by multiple point analysis on the same lysosomes (4). Again, the elements present in this material were assumed to be homogeneously distributed.

In the present paper the percentage of the area occupied by the elements iron - naturally present -, and cerium - deposited after a cytochemical reaction -, and the relative orientation of the two elements in hepatic lysosomal structures of a patient with idiopathic hemochromatosis was studied by reduced raster X-ray microanalysis before and after treatment by phlebotomy.

Morphometric data on the lysosomal populations were simultaneously acquired. Moreover, a method was proposed for calculating the iron concentration per pixelpoint from the acquired net intensity distribution maps.

Materials and Methods

Liver biopsy material was obtained from a patient with idiopathic hemochromatosis, a condition in which hepatic iron storage is evident. With informed consent, biopsies were performed before and after treatment of the disease by phlebotomy.

After fixation and washing, the tissue was incubated in media to detect acid phosphatase activity with cerium as the capture ion (7). For contrast enhancement a postfixation step with $OsO_4/K_4Ru(CN)_6$ was included (6). After processing for conventional electron microscopy, the tissue blocks were coembedded with 11.5% w/w Fe loaded chelex ion exchange beads (5). Unstained ultrathin sections were mounted on one hole, pioloform-film covered, carbon coated, golden grids and placed in a low-background beryllium specimen holder. The preparations were analysed in a Philips EM 400 analytical microscope, operating at 80 kV with a lanthanum hexaboride source installed. The microscope was equipped with an annular backscattered electron detector, a STEM detector, and a TN 2000 microanalysis system. For the performance of the digital-controlled raster (= scanning area) analyses, a TN 1310 unit was added to the computer system. Within this unit the electron beam can be directed by computer control over the specimen in a line or raster pattern. A colour screen assisted in the visualization of the acquired images and a printer/plotter was used to obtain electron images and X-ray net intensity arrays. For integration of morphometrical (electron image) and chemical (X-ray) data the reduced raster analysis program, as described by De Bruijn (4) was used.

To determine the area of the lysosomal structures in cross-section (hereafter called "area") an electron image was transferred to the STEM screen with a basic magnification of 12,500x, the reduced raster was directed to the structure of interest, and the size of the raster was adapted to the size of lysosomal structure. At 16 x 16 pixelpoints per reduced raster area, an electron image of the reduced raster area was acquired and the area of the lysosomal structure was computed. For simultaneous X-ray mapping three 400 keV wide regions of interest (ROI) were marked in the spectrum acquired by point analysis Fe, Ce, and a peak-free background region (for further details see De Bruijn (4) and De Bruijn et al. (5)). After choosing the spot size (in our study 50 or 100 nm) and condenser II aperture (resp. 150 μ and 50 μ) an appropriate dwell time was determined by performing a line scan in the middle of the reduced raster area (for our material 0.4 sec.). Beam intensity, measured at the level of insulated condenser II aperture, was kept between 0.55 and 0.60 μA. Subsequently the 16 x 16 X-ray net intensity images were acquired for the three pre-set ROIs. Thresholds for the elements Fe and Ce (separating the Fe signals obtained from outside the particle from those inside the particle) were determined in advance. This was done by X-ray mapping an organelle-free part of the cytoplasm, calculating the mean value and the standard deviation of the obtained net intensity values for the two elements and setting the threshold values on the mean plus three times the S D.

The printer/plotter was used for integrating the electron image and X-ray net intensity information and for delineation of the acquired signal for Fe and Ce over the threshold value. In this way the percentage of the area of the lysosomal structure occupied by either, both, or neither of the elements, could be visualized and calculated. Moreover, the relative orientation of both elements could be visualized (Figs. 1-4).

For calculating Fe concentrations per pixelpoint from the obtained net intensity values the following acquisitions were performed under carefully controlled conditions: Fe net intensity X-ray maps of 11.5% Fe loaded chelex ion exchange beads were made with four beam intensities, measured at the level of the insulated C II diaphragm, e.g., 0.076 μA; 0.158 μA; 0.312 μA and 0.580 μA. Simultaneously acquired background X-ray maps were obtained. A spot of 100 nm diameter was chosen and the size of the raster was adapted in such a way that the interpixel distance virtually equalled the spot diameter (109 nm vs 100 nm). A dwell time of 0.4 sec. was used. The same conditions were set for a lysosomal structure in which iron was present, and Fe and background X-ray maps were obtained at the four beam intensities mentioned. Choosing the highest beam intensity (0.580 μA), under the conditions of dwell time, spot diameter and magnification mentioned, Fe, Ce and background X-ray maps were acquired from the hepatic lysosomal structures of the liver tissue obtained before and after phlebotomy treatment.

Results

The data on the measured area of the lysosomes in cross-section, as well as on the relative area occupied by Fe and Ce, before and after phlebotomy, are summarized in Table 1. Phlebotomy appeared to result in a decreased size of the lysosomal structures and in an increase of the relative area occupied by Ce.

Before phlebotomy, iron was homogeneously distributed over the lysosomal area and cerium, if present, randomly dispersed (Fig. 4). After phlebotomy, four more patterns of relative elemen-

TABLE 1

EFFECT OF PHLEBOTOMY ON HEPATIC LYSOSOMES

	BEFORE PHLEBOTOMY	AFTER PHLEBOTOMY
MEAN AREA (μm^2)	16.45 ± 9.8	0.65 ± 0.83•
RANGE (μm^2)	0.47 ± 35.25	0.08 ± 5.60
NO OF LYSOSOMES ANALYSED	27	50
AREA OCCUPIED BY FE (%)*	91 ± 13	64 ± 32•
AREA OCCUPIED BY CE (%)*	6 ± 9	70 ± 29•

* Mean ± SD
• Significantly different ($p < 0.01$) from the situation before phlebotomy (Mann-Whitney U-test)

TABLE 2

REDUCED RASTER ANALYSIS OF AN 11.5% W/W IRON CHELEX ION EXCHANGE BEAD AT 16 X 16 PIXELPOINTS

BEAM INT. μA	FE COUNTS* $\bar{x}\pm SD$	BACKGR. COUNTS* $\bar{x}\pm SD$	FE/BGp• $\bar{x}\pm SD$	FE/BGm+ $\bar{x}\pm SD$
0.580	226.6±23.6	30.1±5.6	7.5±1.9	7.6±0.6
0.312	192.5±17.3	25.0±5.2	7.6±2.2	7.7±0.7
0.158	127.6±18.6	17.3±3.9	7.1±2.5	7.3±1.1
0.076	78.1±14.9	10.5±3.4	6.9±3.6	7.4±1.4

* Per pixelpoint per 0.4 sec.
• Mean ratio: FE per pixelpoint to background per pixelpoint
\+ Mean ratio: FE per pixelpoint to mean background

tal orientation could be distinguished (Figs. 5-8).

Mean Fe net intensity values, mean background values and and mean peak to background ratio values of 11.5% w/w iron loaded chelex beads at four beam intensities are presented in Table 2.

Mean peak to background ratio values of this standard were calculated in two ways: (i) the Fe net intensity values per pixelpoint were divided by the background value belonging to that particular pixelpoint and averaged over 256 pixel points (= mean Fe/BGp) and (ii) the Fe net intensity values per pixelpoint were divided by the mean background value and averaged over 256 points (= mean Fe/BGm).

From these figures it was concluded that 11.5% w/w iron is presented best by a peak to background value of 7.5. Accordingly the conversion factor to absolute iron concentration (in % w/w) was set on 1.6.

Fe net intensity values, background values and peak to background ratio values per pixelpoint of an iron containing structure at the same four beam intensities are presented as distribution histograms in Figs. 9 - 12. Peak to background ratio values per pixelpoint (Fe/BGp and Fe/BGm) were calculated in the same way as described for the standard, but not averaged. Only those values lying within the Fe X-ray image are shown in the histograms (Figs. 9 - 12).

Finally, 40 lysosomal structures (20 before and 20 after treatment, respectively) were analysed under the condition: interpixel distance equals spot diameter.

From these 20 lysosomal structures 10 were chosen situated in one hepatocyte (Figs. 13-16, nrs. 1-10) and 10 were chosen at random (Figs. 13-16, nrs 11-20). Absolute w/w iron concentrations per pixelpoint per lysosomal structure were calculated by multiplying the Fe/BGp and the Fe/BGm ratio values by the conversion factor of 1.6. From these values the lowest, mean, and highest concentrations per lysosomal structure are presented in Figs. 13-16.

Discussion

In our biological material, i.e., lysosomal structures of a patient with idiopathic hemosiderosis, we encountered two elements: the naturally present iron (in the ferritin/hemosiderin form) and the introduced cerium (a capture ion detecting the presence of acid phosphatase). From conventional transmission electron micrographs it became evident, that these organelles displayed a heterogeneous distribution of one or both elements. Moreover, it was demonstrated (by EPMA) that phlebotomy treatment could influence not only the iron content of these organelles, but their acid phosphatase activity as well (Cleton et al. submitted for publication). The reduced raster program (4), integrating morphometrical (electron-image) and chemical (X-ray) information, enabled us to acquire simultaneously data about the size of the area of a lysosomal structure, the relative orientation of iron and cerium inside the organelle, and the concentration of these elements in the lysosomal structure and in the surrounding cytoplasm.

As is known from semiquantitative determinations (1), the amount of iron in the liver decreases after phlebotomy treatment.

As is evident from Table 1, in the ultrathin section, the area of the lysosomal structures is substantially smaller after phlebotomy treatment than before. Moreover, the percentage of the lysosomal area, occupied by iron, averaging 91% before treatment, decreases after phlebotomy (Table 1). On the other hand, the percentage of the surface area, occupied by cerium, increases significantly (Table 1). Moreover, the presence of acid phosphatase in all iron containing structures after phlebotomy comfirmed previous results.

These observations, combined with the data on the relative orientation of the two elements after phlebotomy treatment (Figs. 4 - 8) induced

ORIGINAL IMAGE: VIDEO
OVERLAY IMAGE: VIDEO
MAGNIFICATION: 102400
LABEL:8-8-85/V16/LY3

OVERLAY THRESHOLD: 141
TOTAL AREA: 1490116 NM^2

NUMBER OF POINTS (I.P.): 46
MEAN (I.P.): 200.29
S. DEVIATION (I.P.): 45.50
MEAN+2S.D. (I.P.): 291.129 C/P
DEGREES OF FREEDOM: 254
DWELL-TIME/POINT: 1000000 /USEC.
SPOTAREA: 1963 NM^2
INTER PIXEL DISTANCE: 76 NM

NUMBER OF POINTS (O.P.): 210
MEAN (O.P.): 96.32 C/P
S. DEVIATION (O.P.): 13.30 C/P
MEAN+2S.D. (O.P.): 122.92 C/P
P 0.05

ANALYSED AREA: 33.73 %
AREA (I.P.): 267774 NM^2

114	111	102	103	123	93	76	77	99	105	102	117	102	90	94	110
96	83	117	98	91	93	84	101	100	110	96	106	87	71	105	108
109	85	109	122	104	110	110	87	101	100	113	114	115	94	97	104
78	103	105	92	127	81	97	96	100	110	109	93	102	94	104	103
72	103	107	96	97	155	165	110	93	80	111	97	92	100	88	89
74	106	141	159	168	251	233	94	92	83	96	71	110	81	76	93
80	147	147	153	252	254	209	92	97	96	94	93	103	89	102	93
98	106	149	247	255	247	249	152	120	93	96	90	89	80	92	81
85	157	165	254	255	255	235	110	99	104	100	98	74	57	78	89
80	94	161	253	255	255	206	189	113	111	96	96	84	99	83	87
100	108	141	253	255	255	190	92	128	97	90	98	84	92	103	96
88	97	96	208	217	237	78	91	102	72	104	76	96	78	71	92
93	110	79	145	165	167	142	107	122	84	100	110	97	72	74	84
107	110	146	160	107	153	111	77	92	103	70	79	108	110	97	90
96	118	100	112	114	74	76	93	71	124	108	91	101	105	92	77
109	102	98	110	103	108	74	71	110	125	104	75	79	108	100	127

Fig. 1. Electron image of a lysosome in cross section. Threshold 141 superimposed.

ORIGINAL IMAGE: XRAY FE
OVERLAY IMAGE: XRAY FE
MAGNIFICATION: 102400
LABEL:8-8-85/X16/LY3

OVERLAY THRESHOLD: 9
TOTAL AREA:1490116 NM^2

NUMBER OF POINTS (I.P.): 34
MEAN (I.P.): 29.00 C/P
S. DEVIATION (I.P): 18.06 C/P
MEAN+2S.D. (I.P.): 55.12 C/P
DEGREES OF FREEDOM: 254
DWELL-TIME/POINT: 1000000 /USEC.
SPOTAREA: 1963 NM^2
INTER PIXEL DISTANCE: 76 NM

NUMBER OF POINTS (O.P.): 222
MEAN (O.P.): 1.87
S. DEVIATION (O.P.): 2.28 C/P
MEAN+2S.D. (O.P.): 6.43 C/P
P 0.05

ANALYZED AREA: 33.73%
AREA(I.P.): 197887 NM^2

2	0	5	8	0	3	3	0	0	0	0	0	3	0	0	5
4	8	1	8	0	0	1	0	8	1	4	3	2	1	3	3
1	1	0	7	4	1	3	0	3	0	0	0	0	0	0	0
2	4	0	4	5	9	0	0	6	0	0	5	3	0	0	2
2	2	6	7	15	1	0	5	4	0	3	5	0	0	4	0
3	6	22	83	59	9	6	0	2	0	2	0	0	0	0	5
4	14	31	55	15	7	11	4	0	3	0	1	2	0	1	1
3	1	42	41	55	20	23	0	0	0	3	9	0	0	0	2
3	6	38	41	15	38	31	2	0	3	2	0	4	0	0	0
0	8	42	25	22	22	43	5	0	7	0	0	2	0	0	0
7	3	55	17	27	19	4	0	2	5	0	0	3	0	2	1
3	0	10	10	11	6	10	0	2	2	0	5	0	0	2	0
2	3	7	4	2	1	0	0	6	6	0	2	0	0	2	0
1	0	0	5	2	0	2	0	0	2	2	0	0	0	7	1
2	7	0	0	0	0	0	0	0	0	4	0	0	2	1	1
0	1	3	0	2	2	7	0	2	0	2	2	0	0	3	4

Fig. 2. Reduced raster Fe X-ray map from the same particle. Threshold 9 superimposed.

ORIGINAL IMAGE: XRAY CE
OVERLAY IMAGE: XRAY CE
MAGNIFICATION: 102400
LABEL:8-8-85/X16/LY3/

OVERLAY THRESHOLD: 10
TOTAL AREA:1490116 NM^2

NUMBER OF POINTS (I.P.): 37
MEAN (I.P.): 24.57 C/P
S. DEVIATION (I.P.): 11.90 C/P
MEAN+2S.D. (I.P.): 48.73 C/P
DEGREES OF FREEDOM: 254
DWELL-TIME/POINT: 1000000 /USEC.
SPOTAREA: 1963 NM^2
INTER PIXEL DISTANCE: 76 NM

NUMBER OF POINTS (O.P.): 219
MEAN (O.P.): 3.68 C/P
S. DEVIATION (O.P.): 2.96 C/P
MEAN+2S.D. (O.P.): 9.62 C/P
P 0.05

ANALYZED AREA: 33.73%
AREA (I.P.): 215322 NM^2

2	0	2	5	2	1	3	0	2	0	7	0	2	4	2	7
7	1	2	7	2	6	2	0	6	1	7	9	7	3	3	6
2	1	6	6	2	2	7	0	3	0	2	0	6	0	6	0
2	1	7	4	2	8	2	0	11	3	2	2	10	1	2	3
2	1	6	6	14	0	2	4	2	1	7	11	0	4	2	2
7	5	11	14	14	3	18	2	3	0	6	0	7	10	7	1
6	13	22	15	26	11	15	2	2	8	2	7	11	0	3	10
3	0	18	27	30	23	23	6	3	6	2	9	3	0	3	6
2	8	31	39	51	36	39	10	7	3	2	2	2	0	3	6
2	9	30	45	39	26	31	9	3	9	3	7	2	7	2	0
2	5	11	46	42	25	10	0	3	5	6	7	7	6	2	5
7	0	19	37	27	6	10	6	7	1	7	7	7	3	4	0
2	2	6	8	11	3	2	7	3	5	3	0	3	4	2	0
3	0	6	4	6	4	2	0	14	1	2	5	2	7	6	1
2	0	3	5	3	0	3	4	10	0	2	11	7	4	2	4
0	2	2	0	2	1	2	0	3	0	2	11	3	6	2	1

Fig. 3. Reduced raster Ce X-ray map from the same particle.
Threshold 10 superimposed.

us to suggest a possible sequence of events: By an unknown process, triggered by the demand for iron, cerium (acid phosphatase) negative, iron containing organelles either break up into smaller units or release iron (ferritin, hemosiderin). Subsequently primary, acid phosphatase positive lysosomes either fuse with these units or take up the released iron (compounds) to form the secondary lysosomes as visualized in Figs. 5 - 8.

In a recent study, using multiple point analysis (4), evidence was presented for a decrease in mean net intensity values for iron after phlebotomy treatment. However, in this study the heterogeneity of the elemental distribution in the lysosomal structures was deliberately ignored.

In our present study, 40 lysosomal structures were analysed in a reduced raster of 16 x 16 pixelpoints, to get an impression of the iron concentration per pixelpoint. As the chosen interpixel distance virtually equalled the size of the spot diameter, 70% of the area in cross section of the lysosomal structure was analysed. When beam broadening is taken into account, the percentage will approximate 100. Instrumental conditions were tested on iron loaded chelex beads and carefully controlled. However, the problem of variation in the beam intensity emitted by the LaB_6 source during a time-consuming analysis of 40 lysosomal structures had to be coped with. Therefore a ratio program was incorporated into the reduced raster program (De Bruijn et al.,submitted for publication). In this

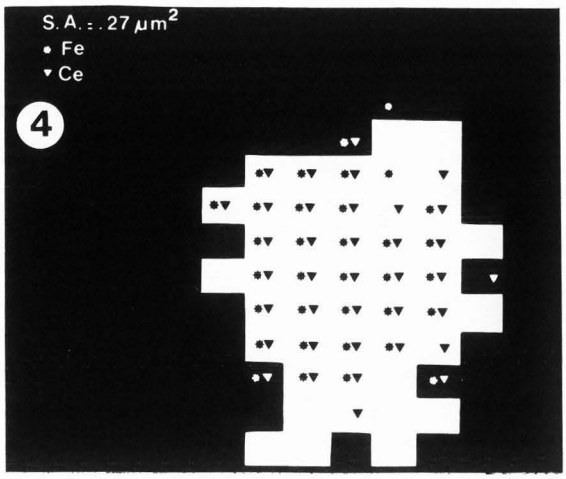

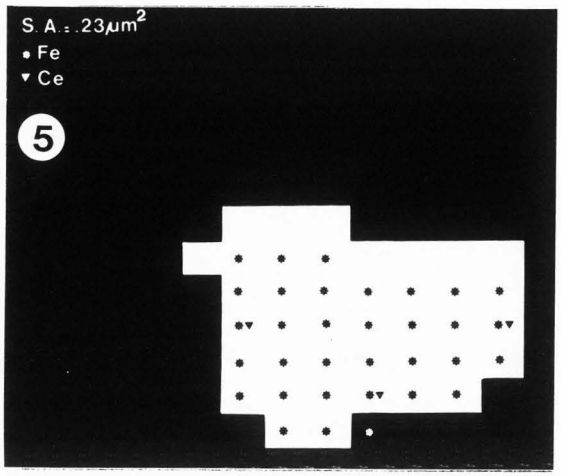

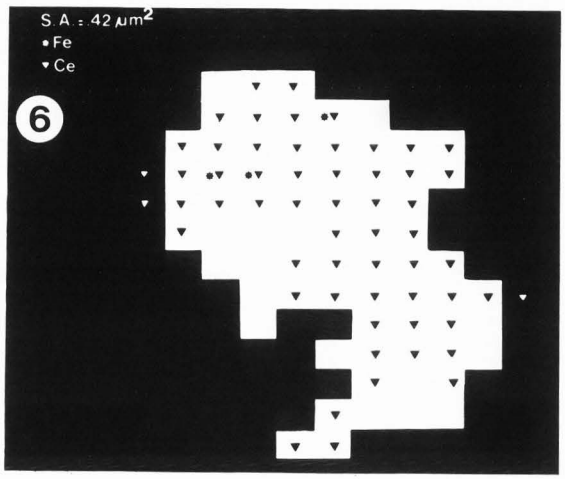

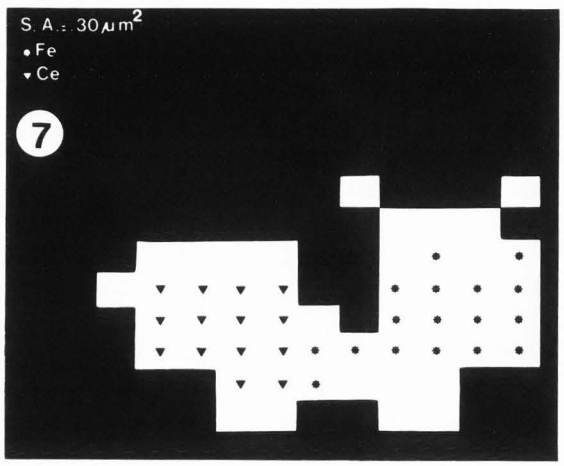

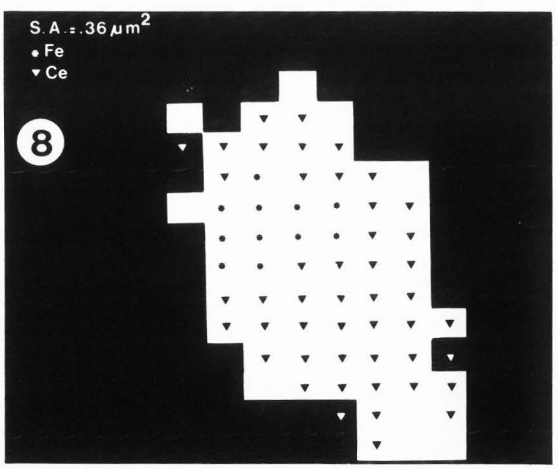

Fig. 4. Composition of the three overlay figures; giving the precise elemental loci of Fe and Ce.

Fig. 5. Determination of cross-sectioned area (S.A.) and elemental distribution at 16 x 16 pixelpoints in a hepatic lysosome after phlebotomy treatment.
Some cerium is randomly dispersed.

Fig. 6. Determination of cross-sectioned area (S.A.) and elemental distribution at 16 x 16 pixelpoints in a hepatic lysosome after phlebotomy treatment.
Some iron is randomly dispersed.

Fig. 7. Determination of cross-sectioned area (S.A.) and elemental distribution at 16 x 16 pixelpoints in a hepatic lysosome after phlebotomy treatment. Iron and cerium in different parts of the lysosome.

Fig. 8. Determination of cross-sectioned area (S.A.) and elemental distribution at 16 x 16 pixelpoints in a hepatic lysosome after phlebotomy treatment. Cerium surrounds an iron "nucleus".

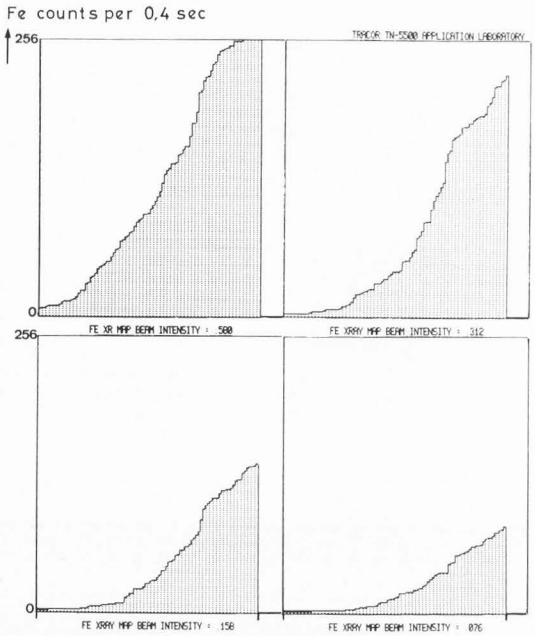

Fig. 9. Distribution histograms of Fe net intensity X-ray values per pixelpoint (y-axis) of a lysosome at four beam intensities. The Fe X-ray values are arranged in order of increasing intensity along the x-axis.

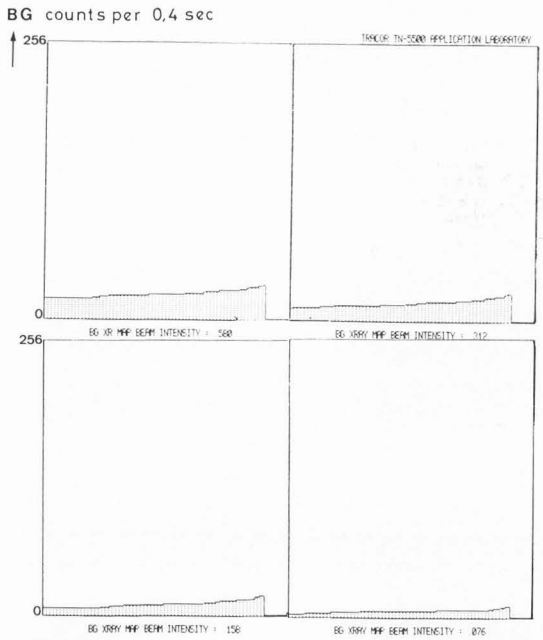

Fig. 10. Distribution histograms of background (BG) values per pixelpoint (y-axis) of the same lysosome at four beam intensities. The background values are arranged in order of increasing intensity along the x-axis.

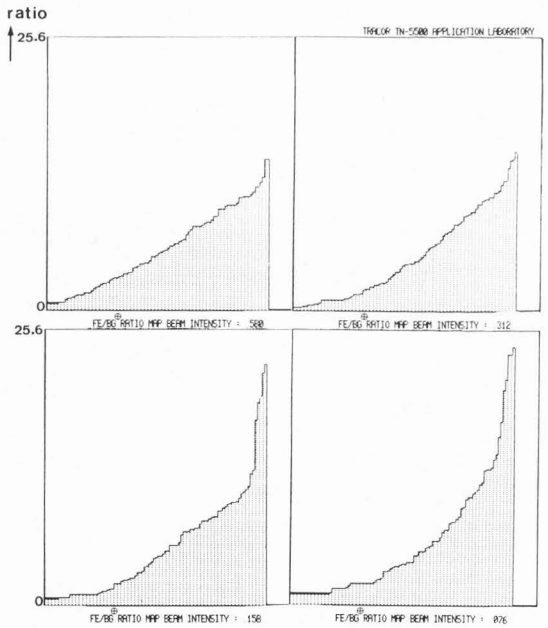

Fig. 11. Distribution histograms of the ratios: Fe net intensity values per pixelpoint to background values per pixelpoint (Fe/BGp: y axis)of the same lysosome at four beam intensities. The ratio values are arranged in order of increasing magnitude along the x-axis.

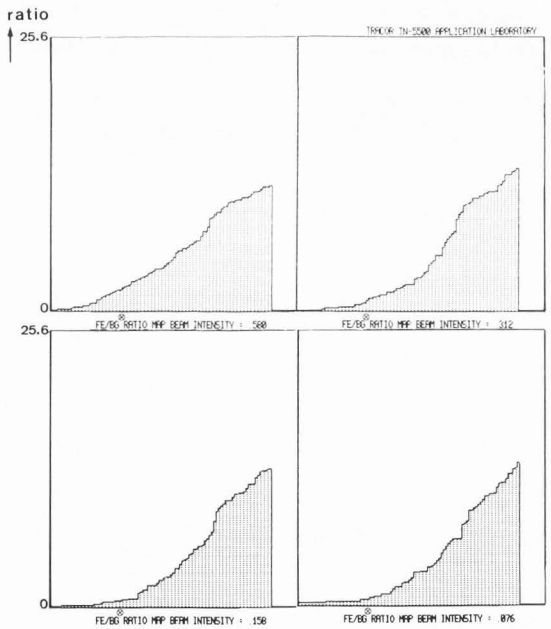

Fig. 12. Distribution histograms of the ratios: Fe net intensity values per pixelpoint to mean background values (Fe/BGm: y-axis) of the same lysosome at four beam intensities.
The ratio values are arranged in order of increasing magnitude along the x-axis.

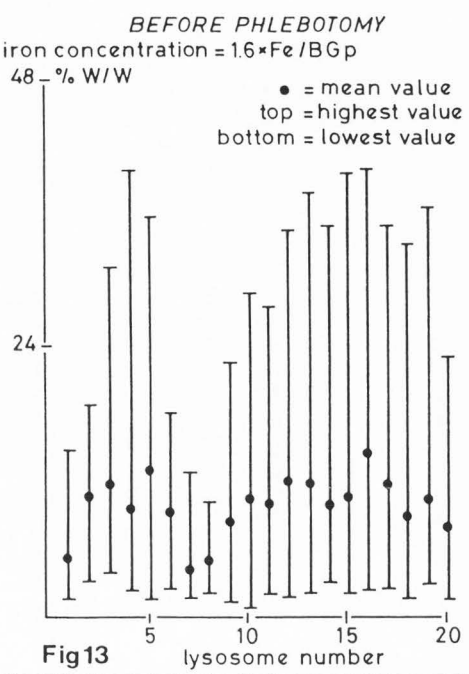

Fig 13

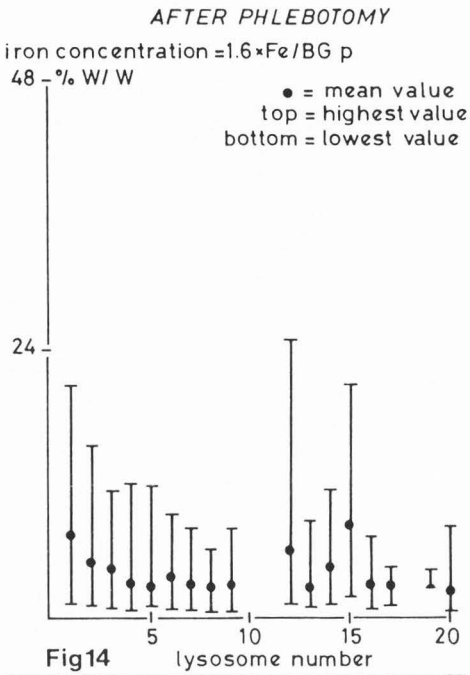

Fig 14

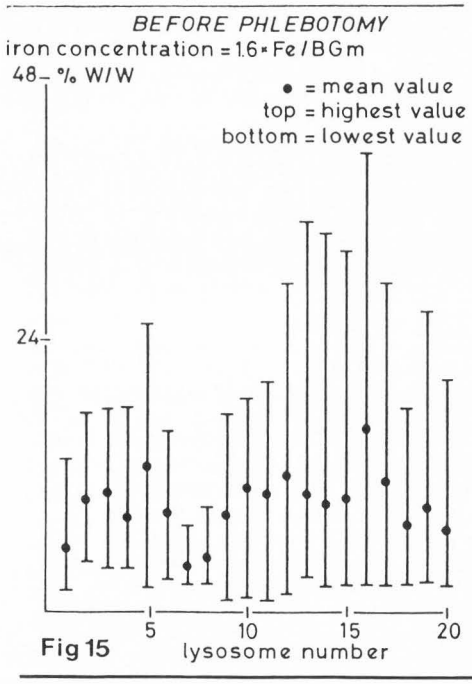

Fig 15

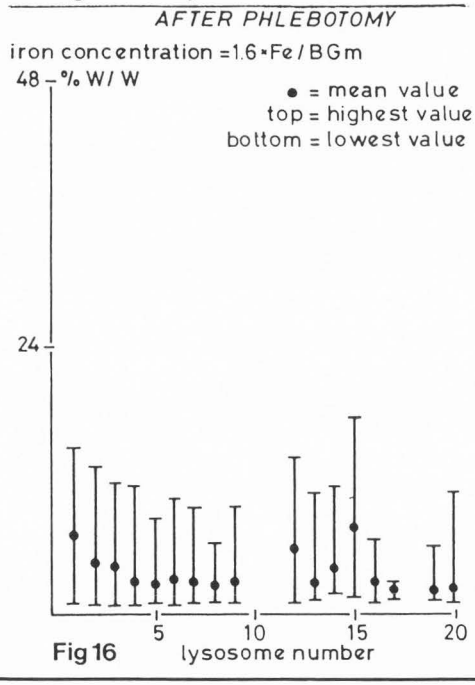

Fig 16

Figs. 13-16: Number of lysosomes before (Figs. 13 & 15) and after phlebotomy (Figs. 14 & 16) for background calculated per pixel (Figs. 13 & 14) and as mean of all pixels (Figs. 15 & 16).

way two ratio arrays for 11.5% w/w iron loaded chelex beads were obtained (Fe/BGp and Fe/BGm), as described in Materials and Methods.

Of this homogeneous material mean ratios were calculated at four different beam intensities (Ib). The mean ratios, calculated either way, were independent of Ib, and a factor, converting ratio to absolute (% w/w) iron concentration could be calculated.

The same procedure for calculating the Fe/BGp and the Fe/BGm per pixelpoint (see Materials and Methods) was followed for an at random chosen lysosomal structure in which various iron concentrations could be expected. Theoretically, the shape of the distribution histograms of the peak to background values (Figs. 11 and 12) should be independent of Ib. Whereas this appears to be true for the Fe/BGM ratio (Fig. 12) where only a small deviation at low ratio values (corresponding to low Fe intensities) is seen, this is not the case for the Fe/BGp ratio (Fig. 11). At low beam currents, marked deviations both at the low ratio value end and at the high ratio value end (low values of BGp) are noted (Fig. 11c,d). Both types of deviations are due to statistical fluctuations at low count rates for characteristic or background counts, respectively. This effect is, of course, more severe in the case of the BGp ratio. A similar conclusion can be drawn from the experiment

described in Table 2. As expected, the standard deviation increased with decreasing beam intensity, and was generally larger with BGp that with BGm. Both phenomena can be attributed to statistical factors. Counting statistics are poor at low beam intensities, and the value for background intensity of a single pixelpoint (BGp) carries a much larger statistical uncertainty than the calculated mean of those values (BGm).

Although it is theoretically more correct to use BGp-values, this has to be weighed against the poor counting statistics. At high beam intensities, the use of BGp may be well possible. In Figs. 13-16, therefore, both Fe/BGp and Fe/BGm were converted to iron concentrations.

The differences in calculated iron concentrations before and after phlebotomy treatment are remarkable (cf. Figs. 13-16).

In conclusion we can state that the results of the reduced raster analysis are in agreement with our previous study by multiple point analysis: after phlebotomy treatment the overall absolute iron concentration of the individual lysosomal structures is markedly lower than before treatment by phlebotomy.

Acknowledgements

We thank the Utrecht Foundation for Blood Research (SOBU) for financial support and Dr. J.J.M. Marx (Department of Haematology, University Hospital Utrecht) for providing the patient material.

References

1. Barry M. (1974) Progress report. Iron and the liver. Gut 15, 324-334.

2. Cleton MI, Sindram JW, Rademakers LHPM, Zuyderhoudt FMJ, De Bruijn WC, Marx JJM. (1986) Ultrastructural evidence for the presence of ferritin-iron in the biliary system of patients with iron overload. Hepatology 6, 30-35.

3. Cleton MI, Frenkel EJ, De Bruijn WC, Marx JJM. (1986) Determination of iron to phosphorus ratios of iron storage compounds in patients with iron overload. A chemical and electron probe X-ray analysis. Hepatology, In Press.

4. De Bruijn WC. (1985) Integration of X-ray microanalysis and morphometry of biological material. Scanning Electron Microsc. 1985; II: 697-712.

5. De Bruijn WC, Cleton MI.(1985) Application of chelex standard bead in integrated morphometrical and X-ray microanalysis. Scanning Electron Microsc. 1985; II: 715-729.

6. De Bruijn WC, Van Buitenen JHM. (1981) X-ray microanalysis of aldehyde fixed glycogen contrast-stained by Os(VI) Fe(II) and Os(VI) Ru(IV) complexes. J. Histochem. Cytochem. 28, 1242-1250.

7. Hulstaert CE, Kalicharan D, Hardonk MJ. (1983) Cytochemical demonstration of phosphatases in the rat liver by a cerium based method in combination with osmium tetroxide and potassium ferrocyanide postfixation. Histochem. 78, 71-79.

Discussion with Reviewers

K. Zierold: Could variation in the local Fe- and Ce concentrations in the lysosomes be caused by preparation-induced segregation?
Authors: With regard to our iron containing compounds we cannot absolutely exclude preparation induced segregation after aldehyde fixation. However, if this was true for the iron compounds in the lysosomal structures we would have expected this phenomenon to occur in the cytoplasm as well. In fact, the cytoplasmic ferritin is usually found as freely dispersed particles and only occasionally a cluster is observed. Hemosiderin, which is insoluble, is thought to be a ferritin polymer or a lysosomal ferritin degradation product. It is not likely to segregate under the influence of aldehyde fixatives. With regard to the cerium: this element is introduced and deposited after fixation.

K. Zierold: How do you determine criteria for the most appropriate analysis conditions such as beam intensity, number of pixel points, measuring time etc?
Authors: We determined criteria for the most appropriate analysis conditions by using ion exchange beads as a reference as described previously by De Bruijn (ref. 5).

K. Zierold: Do your sections undergo radiation damage-induced alterations during analysis?
Authors: Radiation damage is unavoidable. However, with the reduced raster analysis at 16 x 16 pixelpoints the dwell time per pixelpoint is much shorter than in conventional point analysis. This reduces considerably mass loss as well as mass gain.

Reviewer II: Are there any clinical indications that motivate such an extensive investigation on a patient?
Authors: It had been decided to follow in liver biopsy material the effects of phlebotomy treatment in a group of patients with hemosiderosis. In this way a comparison could be made between a semiquantitative iron gradation (Perls' blue staining, graded according to Scheuer) and obtained hematologic and biochemical data. In the material that became available we decided to investigate with a high resolution technique the iron content per individual lysosomal structure as well as other cell biological aspects such as lysosomal enzyme activity.

Reviewer II: You apparently omit correction for extraneous background. Doesn't this affect the accuracy of your measurements?
Authors: We omitted correction for extraneous background because we compared the calculated peak to background ratios of the unknown with a peak to background ratio obtained from a standard which was present in the same ultrathin section. We presumed that the contribution of the extraneous background would be rather similar for both measurements and that, although the precision of our measurements might be affected, our accuracy is not.